Research Article

Dual effect of MgS addition on li_2s ionic conductivity and all-solid-state Li–S cell performance

Nguyen Huu Huy Phuc[1] · Maeda Takaki[1] · Hikima Kazuhiro[1] · Muto Hiroyuki[1] · Matsuda Atsunori[1]

Received: 1 July 2020 / Accepted: 29 September 2020 / Published online: 9 October 2020

Abstract
The effect of a multivalence cation, i.e. Mg^{2+}, on both the ionic conductivity of $Li_{2-2x}Mg_xS$ ($0.05 \le x \le 0.2$) and the all-solid-state Li–S cell performance employing $Li_{2-2x}Mg_xS$ as an active material is investigated. MgS was added to Li_2S ($Li_{2-2x}Mg_xS$) using the planetary ball milling method. No trace of MgS was detected by X-ray diffraction (XRD) with $x \le 0.05$. Improvement of the ionic conductivity upon addition of MgS was observed even in the samples with $0.05 \le x \le 0.2$, where the remaining MgS was detected by XRD analysis. Vacancy formation and the nanoionic effect were the governing factors for Li^+ conduction. Stabilization of the cycle capacity was also achieved in the cell containing $Li_{1.7}Mg_{0.15}S$ when compared with that employing bare Li_2S as the electrode active material. Improvement of the ionic conductivity by approximately 2 orders of magnitude at 90 °C was obtained with $x = 0.15$ compared with that with $x = 0$. In addition, the charge–discharge capacities of the cell with $x = 0.15$ were stable up to 50 cycles, while the cell with $x = 0$ began to degrade after the 25th cycle.

Keywords Lithium–sulfur battery · Li–S battery · Li_2S conductivity

1 Introduction

Elemental sulfur has been attracting much interest from researchers owing to its use as an active material in lithium and sodium rechargeable batteries. This interest has resulted from its abundance and high theoretical capacity of approximately 1670 mAh g^{-1} [1–4]. Batteries that employ S/Li_2S are faced with many issues that arise directly from the materials such as low conductivities and large volume changes in the cycling process. Employing elemental sulfur as an active material results in the presence of either Li metal or pre-lithiated materials at the anode, which then result in other problems to be solved. The Li–S battery, with Li metal at the anode, resembles other Li metal batteries, where the problems at the anode become evident above a certain current density or areal capacity. To date, the Li metal battery, which is the holy grail of electrochemical technology, is still insufficient to satisfy commercial requirements because the stripping–plating process of Li ion on Li metal is yet to be fully controlled [5]. The use of Li_2S as a cathode active material has opened the door to many other commercially available anode materials like carbonaceous materials or silicon. Either hard or soft carbon is obviously more favorable than lithium metal in terms of lithium-ion storage, and their durability and safety have been proven over many years. However, a Li_2S–carbonaceous materials/silicon battery is expected to

Electronic supplementary material The online version of this article (https://doi.org/10.1007/s42452-020-03604-2) contains supplementary material, which is available to authorized users.

✉ Nguyen Huu Huy Phuc, nguyen.huu.huy.phuc.hr@tut.jp; ✉ Matsuda Atsunori, matsuda@ee.tut.ac.jp; Maeda Takaki, maeda.takaki.px@tut.jp; Hikima Kazuhiro, hikima@ee.tut.ac.jp; Muto Hiroyuki, muto@ee.tut.ac.jp | [1]Department of Electrical and Electronic Information Engineering, Toyohashi University of Technology, 1-1 Hibarigaoka, Tempaku, Toyohashi, Aichi 441-8580, Japan.

have a lower energy density than one employing lithium metal [6, 7].

As the ionic and electronic conductivities of S and Li_2S are extremely low at room temperature, improvement of these properties is required as a priority to be able to employ them as battery active materials [7]. The electronic conductivity is usually enhanced by the introduction of carbon-based electrically conductive materials, such as carbon nanotubes, reduced graphene oxide, ketjen black (KB) and so on [4, 8–10]. The boosting of the intrinsic ionic conductivity of Li_2S and its application in a battery has almost been completely overlooked until recently. T. Hakari et al. observed an increase of the Li^+ conductivity in Li_2S–LiX (X = I^-, Br^-, Cl^-) and reported the superior performance of batteries that employed these as active materials even though the electrode ionic and electronic conductivities were further enhanced by the addition of both a solid electrolyte and vapor-grown carbon fiber [11]. A systematic study of Li^+ transport in Li_2S, conducted by S. Lorger et al., led to the conclusion that the ion conduction is governed by Frenkel disorder and vacancy–dopant association [12]. Density functional theory calculations were employed to stimulate the effect of transition metal doping on the Li_2S properties, and it was found that Fe doping resulted in a reduction of the Li vacancy formation energy and the induction of a gap state, which then resulted in the accommodation of an electron during extraction / insertion of a Li ion [13]. We have previously reported that a slightly reduced amount of Li_2S in $Li_7P_2S_8I$ results in an increase of the ionic conductivity owing to the formation of a lithium vacancy structure [14, 15].

Inspired by the abovementioned findings, we noted that the effect of a multivalence cation dopant on the ionic conductivity of Li_2S and the properties of a Li_2S-based electrode has yet to be reported, especially in the field of all-solid-state batteries. Therefore, this study aims to investigate the change in ionic conductivity of Li_2S upon addition of MgS, and the differences in the all-solid-state cell performance with and without the addition of MgS to the positive electrode active materials. Ionic conductivity modification was observed in $Li_{2-2x}Mg_xS$ ($0 \le x \le 0.2$), and the highest conductivity was detected in the sample with $x = 0.15$. Furthermore, superiority in the cycling performance upon addition of MgS was observed but the reason for this will be determined in further studies.

2 Experimental

Li_2S (99.9%, Mitsuwa), P_2S_5 (99%, Merck), LiCl (99.99%, Wako Fuijifilm) and MgS (99.9%, Kojundo Laboratory) were used as received.

$Li_{2-2x}Mg_xS$ ($0 \le x \le 0.2$) samples were prepared by the planetary ball milling method. Li_2S and MgS were mixed for 10 min using an agate pestle and mortar prior to transfer into a 45-mL zirconia pot with zirconia balls (10 mm, 15 balls). The pots were rotated at 500 rpm for 12 h using a Pulverisette 7 (Fritsch) micromill. The obtained samples were recovered and used without any further heat treatment.

Argyrodite-type $Li_{5.5}PS_{4.5}Cl$ was prepared by ball milling following by heat treatment at 440 °C for 2 h in an Ar atmosphere. In a typical batch, Li_2S, P_2S_5 and LiCl were mixed for 10 min using an agate pestle and mortar prior to transfer into a 45-mL zirconia pot with zirconia balls (10 mm, 15 balls). The pot was rotated at 600 rpm for 24 h using a Pulverisette 7 (Fritsch) micromill. The obtained samples were further heat treated at 440 °C for 2 h in an Ar atmosphere. An argyrodite-type structure was confirmed by powder X-ray diffraction (XRD) and its conductivity at room temperature (RT) was approximately 2.8 mS cm^{-1}.

The positive electrode composite was prepared from $Li_{2-2x}Mg_xS$, argyrodite-type $Li_{5.5}PS_{4.5}Cl$ and KB with a weight ratio of 50:40:10 by a ball milling method. The mixture of the three components was introduced into a 45-mL zirconia pot with 4-mm zirconia balls (160 balls). The pots were then rotated at 510 rpm for 10 h to obtain the positive electrode composite.

The structure of the prepared powders was characterized using XRD (Ultima IV, Rigaku). For analysis, the samples were sealed in special holders in an Ar-filled glove box to avoid exposure to air humidity. The morphologies of the prepared composites were characterized using scanning electron microscopy (SEM; JSM 7800F, JEOL) and energy-dispersive X-ray spectroscopy (EDS).

The temperature dependence of the total conductivity of the prepared samples was investigated using alternating-current impedance spectroscopy (SI 1260, Solatron) from 1 MHz to 10 Hz under a dry Ar flow. Prior to the measurements, the samples were pressed into pellets of ~ 10 mm in diameter at a pressure of 550 MPa (at RT). The pellets were then placed in a PEEK holder with two stainless steel rods as blocking electrodes. The cell was placed under an Ar stream in a glass tube for the temperature-dependence measurements. The temperature was gradually increased from room temperature to 150 °C and held at each temperature for 1 h prior to the impedance measurement.

An all-solid-state half-cell was fabricated to investigate the electrochemical performance of the prepared positive electrode composite and solid electrolyte. The prepared argyrodite-type solid electrolyte was employed as a separator, and an In–Li alloy was used as the negative electrode. Indium (In) only can serve as negative electrode in the all-solid-state half-cell using Li_2S as positive electrode

material; however, small amount of Li in In can improve the coulombic efficiency of the cell [16]. Therefore, In–Li alloy was employed as negative electrode in this study. The bilayer pellets (10 mm in diameter), composed of the electrode composite and separator layer (80 mg), were prepared by uniaxial pressing at 550 MPa followed by mounting of indium foil onto the pellets by pressing at 200 MPa. The loading of positive electrode composites in each cell was about 4.2–4.8 mg, in according to loading of Li_2S of 2.1–2.4 mg. The thickness of electrolyte (separator) layer was about 0.80 mm and that of positive electrode was about 0.02–0.03 mm. Two stainless steel rods were employed as current collectors. The electrochemical compatibility of the cell was investigated by cyclic voltammetry (at RT) at a scan rate of 0.1 mV s^{-1} on an SI1287 potentiostat (Solartron). The cells were cycled using a charge–discharge device (BST-2004H, Nagano) in a dry Ar atmosphere. The cutoff voltages were in the range of 3.0–0.60 V versus Li–In at 0.1 C. All the cells were placed in an insulation box that was kept at 30 ± 2 °C for 4 h prior to being tested. Cell preparation was conducted inside an Ar-filled glove-box with $O_2 \le 1.0$ ppm and $H_2O \le 0.1$ ppm.

3 Results and discussion

Figure 1 shows the XRD patterns of the $Li_{2-2x}Mg_xS$ samples prepared by the ball milling method, with Si addition as the internal standard material for peak shift confirmation, and the lattice parameter as a function of x ($0 \le x \le 0.15$). Peaks of MgS were not detected at low loadings up to $x = 0.05$, and their existence was observed at higher addition amounts. However, the structure of Li_2S was still preserved despite the introduction of MgS. A peak shift in the $Li_{2-2x}Mg_xS$ samples was not sufficiently clear in the investigated range of x. It should be noted that the ionic radius of Li^+ (0.59 Å) is close to that of Mg^{2+} (0.57 Å), so a peak shift is hindered as a result [17]. However, the lattice constants as a function of x were calculated and are plotted in Fig. 1b. The lattice constant of $x = 0.05$ was slightly smaller than that of $x = 0$ (ball-milled Li_2S). Further addition of MgS ($x = 0.1$) resulted in the reduction of this value because the ionic radius of Mg^{2+} is slightly smaller than that of Li^+. The sample with $x = 0.15$ had a lattice constant resembling that of the sample with $x = 0.1$, which was in agreement with the remaining MgS that was detected by XRD. This observation may suggest that Mg^{2+} was successfully dissolved into the Li_2S structure to form a $Li_{2-2x}Mg_xS$ solid solution with the limitation at x of nearly 0.1. In fact, the effect of Mg^{2+} doping on Li_2S ionic conductivity was also investigated by Lorger et al., but only a slight improvement of the ionic conductivity was observed [12]. Takeuchi et al. prepared Li_2S–FeS nanocomposites with different molar ratios and applied them to all-solid-state batteries [18]. They found that a solid solution of Li_2S–FeS could be obtained up to a molar ratio of approximately 3:1 by using powder XRD. The lattice parameters were also reported in their study. They found that this value was close to that of bare Li_2S at a low FeS content with a slight reduction observed as the FeS content was increased. Our observation was consistent with these results.

Figure 2a and b shows the temperature dependence of the ionic conductivity, activation energy and pre-exponential factor A of Li^+ conduction of the prepared $Li_{2-2x}Mg_xS$ samples ($0 \le x \le 0.2$). Overall, the presence of MgS in Li_2S resulted in an increase of the ionic conductivity of $Li_{2-2x}Mg_xS$ of approximately two orders of magnitude compared with bare Li_2S, which was also treated by planetary ball milling with similar conditions as those used in the $Li_{2-2x}Mg_xS$ preparation procedure. Because the diameter of Mg^{2+} is similar to that of Li^+ but Mg^{2+} has a higher charge, the increase of ionic conductivity at low MgS loading may be a combination of many other effects, such as cation vacancies, interstitial effects and substitution of Mg^{2+} into Li^+ sites [19]. The remaining MgS in the samples with $x = 0.15$ and 0.20 did not result in a reduction of the conductivity compared with the other samples. It was proposed that the remaining MgS, which was detected by XRD, also contributed to the overall conductivity owing to the nanoionics effect. This enhanced the conductivity at the interface of MgS and Li_2S crystals. Indeed, the activation energy for the movement of Li^+ was slightly reduced when $x = 0.05$ compared with that when $x = 0$. The pre-exponential factor was slightly increased with $x = 0.05$. These results, together with the lattice parameter data, illustrated that a solid solution was formed at $x = 0.05$. Further increase of the MgS content led to drastic changes of the lattice parameter, activation energy and pre-exponential factor. The reduction of both the lattice parameter and activation energy proved that Li^+ ion movement was improved owing to vacancy formation. The reduction of the pre-exponential factor resulted from a decrease of the Li^+ concentration in the $Li_{1.8}Mg_{0.1}S$ solid solution. Despite the limitation for the solid solution formation at a value of x between 0.1 and 0.15, an increase of the ionic conductivity and reduction of the activation energy were observed. Pre-exponential factor A was also slightly increased despite the decrease of the Li^+ concentration at $x = 0.15$. These results, together with XRD pattern and lattice parameter, suggested that Li ion movement in this case was driven by a new mechanism other than vacancy formation because the ionic conductivity was expected to be unchanged or to decrease owing to the remaining MgS in the sample with $x = 0.15$. The sample with $x = 0.2$ exhibited an ionic conductivity slightly lower than that with $x = 0.15$ but still higher than that with $x = 0.1$. In addition,

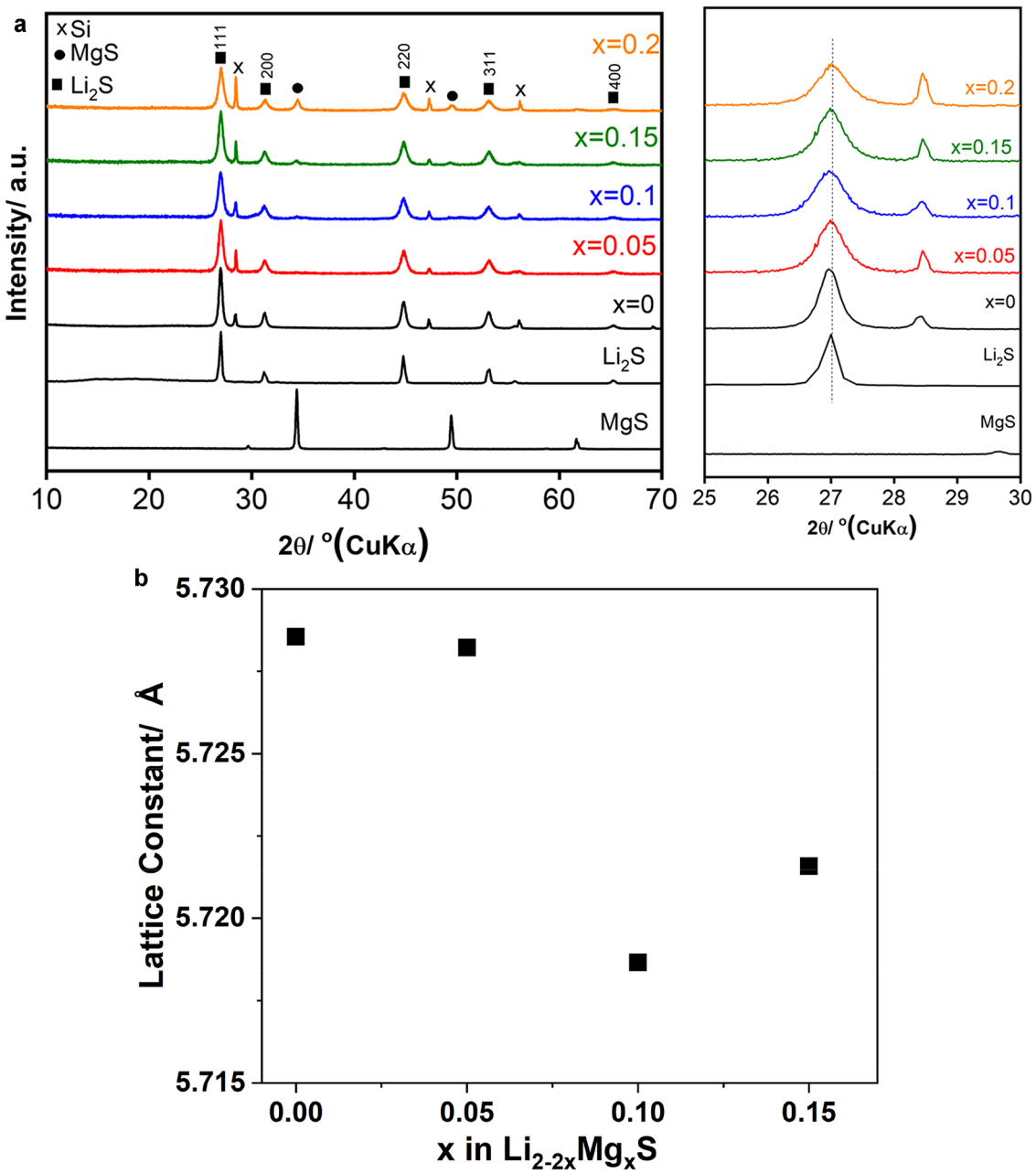

Fig. 1 Structure of $Li_{2-2x}Mg_xS$ prepared by ball milling method. **a** XRD patterns and **b** lattice parameters of $Li_{2-2x}Mg_xS$ samples

the activation energy for the sample with $x = 0.2$ was also lower than that with $x = 0.15$. These results also confirmed the existence of a new conduction mechanism other than vacancy formation. Therefore, the effect of a MgS particle should be noted in this case as the effect of nanoionics was expected to contribute to an improvement of both the ionic conductivities and activation energy for the samples with $x = 0.15$ and 0.2. Upon doping with 4% mol of MgS, a slight increase of the ionic conductivity of Li_2S was observed by Lorger et al. [12]. Recently, nanocomposites of Li_2S and transition metals were prepared by heating mixtures of Li metal and transition metal sulfides at 600 °C [20]. XRD analysis showed the coexistence of both the transition metal sulfide and Li_2S. Li_2S–W and Li_2S–Mo composites exhibited a high ionic conductivity of up to 10^{-4} S cm^{-1} at RT; however, the ionic conductivity of bare Li_2S and its composites with other transition metals was too low to be measured in their study.

Argyrodite-type $Li_{5.5}PS_{4.5}Cl$ was prepared in advance and the SEM–EDS analysis results of its composite with $Li_{1.7}Mg_{0.15}S$ and KB are shown in Fig. 3. P and Cl from the electrolyte, Mg and S from $Li_{1.7}Mg_{0.15}S$, C from KB were

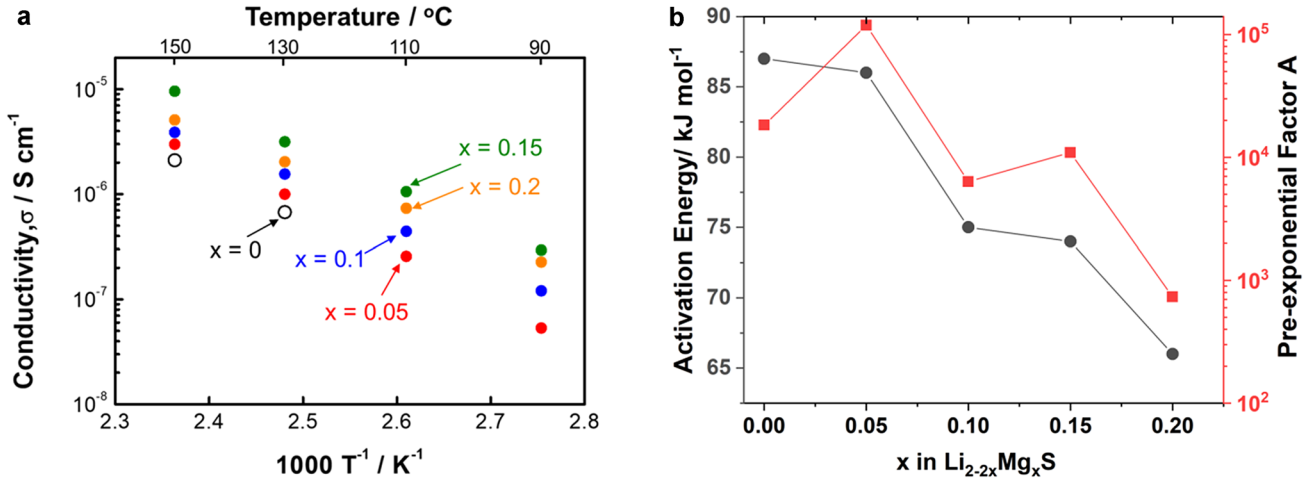

Fig.2 Conduction properties of $Li_{2-2x}Mg_xS$ ($0 \le x \le 0.2$) samples. **a** Temperature dependence of ionic conductivity; **b** Activation energy (closed circle) and pre-exponential factor A (closed square) as function of *x*

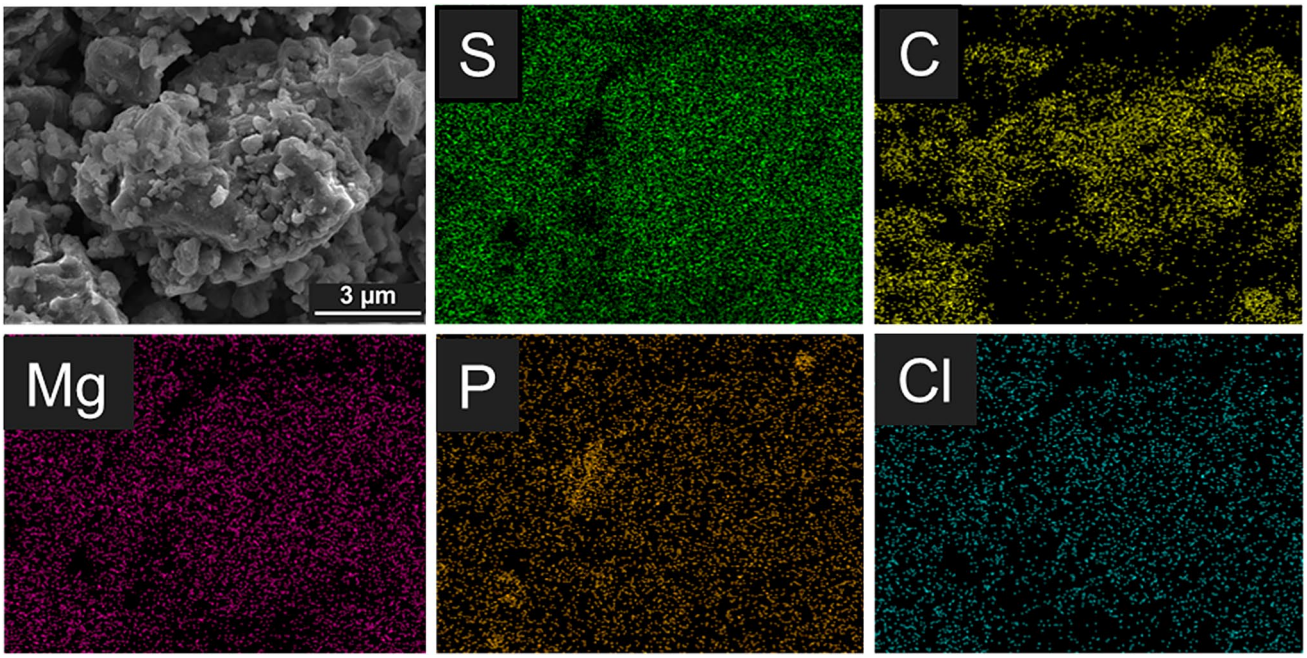

Fig.3 SEM image and EDX mapping result of the electrode composite containing $Li_{1.7}Mg_{0.15}S$, argyrodite solid electrolyte $Li_{5.5}PS_{4.5}Cl_{1.5}$ and Ketjen Black prepared by ball milling method

well detected from EDS analysis. The good distribution of Mg, Cl and C signals in all of the EDS results indicated that the three components of the composite were well-blended together and therefore the conduction paths of both Li^+ and e^- were established. In addition, the EDS signal of P suggested that there were stand-alone solid electrolyte particles. This mapping image seemed to be in good agreement with the SEM observation owing to the existence of particles with different contrasts.

Figure 4 illustrates the electrochemical properties of the all-solid-state cells constructed from the positive composites containing either Li_2S ($x = 0$) or $Li_{1.7}Mg_{0.15}S$ ($x = 0.15$). The cyclic voltammogram of the cell with $x = 0$ and 0.15 (Fig. 4a, b) exhibited only one oxidation peak and two reduction peaks in the range of 0.6–3.0 V vs. Li–In. The oxidation peak at 2.13 V versus Li–In was assigned to the conversion of Li_2S ($Li_{1.7}Mg_{0.15}S$) to S. The two reduction peaks originated from the reaction of S with Li^+ and

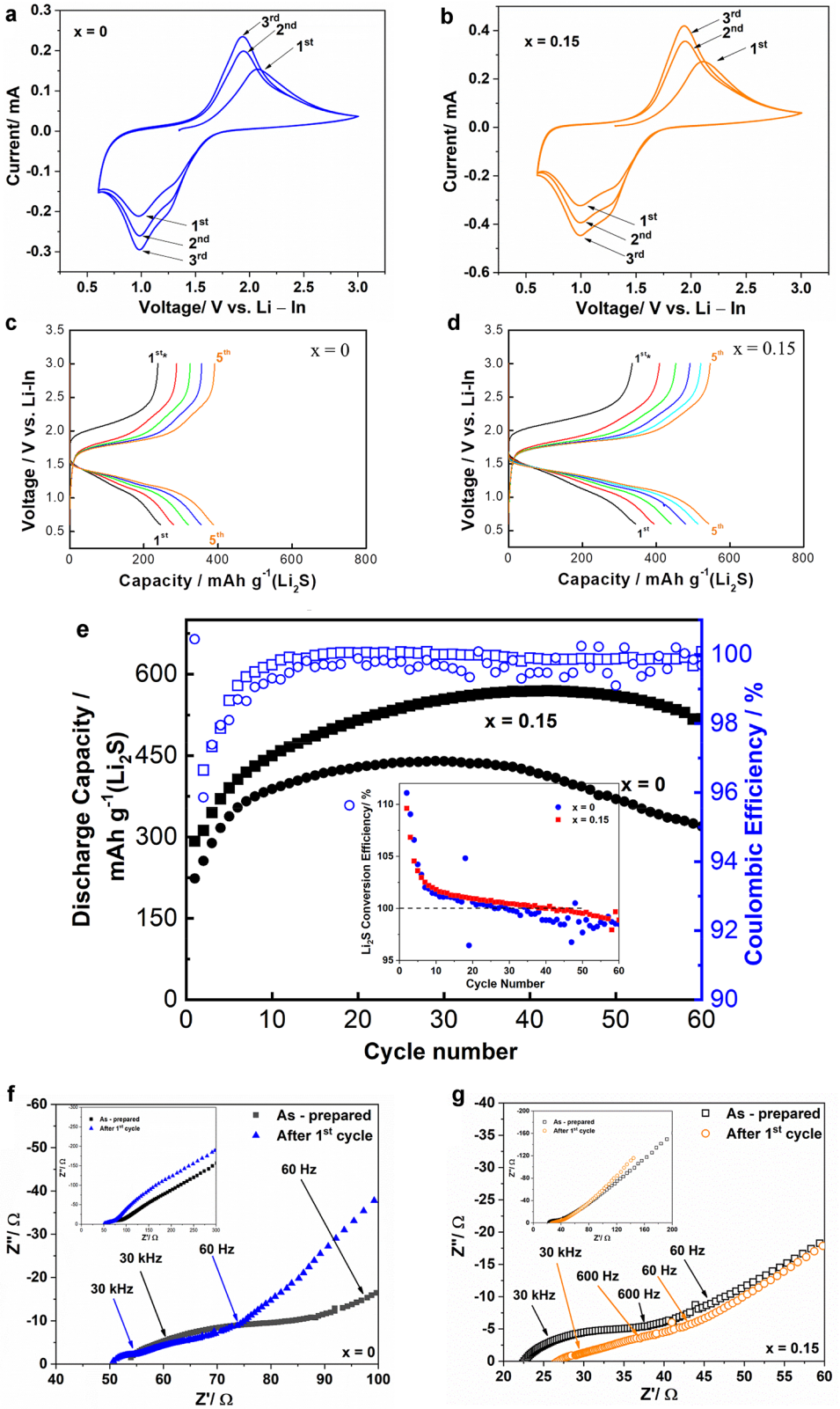

Fig.4 Electrochemical properties of the all-solid-state cell employed the prepared positive electrode composite containing samples $x=0$ and $x=0.15$. **a**, **b** Cyclic voltammogram of the cell with $x=0$ and 0.15, respectively; **c**, **d** voltage profiles of the first 5 cycles of the cell with $x=0$ and 0.15, respectively; **e** cycles performance at 0.1C of all-solid-state cells employed the prepared positive electrode composite containing samples $x=0$ (close circle) and $x=0.15$ (open square) with Li2S conversion efficiency plotted in the small inset; **f**, **g** EIS spectra of all-solidstate cell employed the prepared positive electrode composite containing samples $x=0$ and $x=0.15$ before and after first charge–discharge cycle, respectively

e^- to form Li_2S. In the second cycle, the oxidation peak was slightly shifted to a lower voltage position (1.95 V vs. Li–In) compared with that in the first cycle. The existence of an overvoltage during the first charge cycle of the batteries employing Li_2S as active material has been reported many times despite the use of either liquid or solid electrolytes [21]. Y. Yuan et al. found that the micro-sized Li_2S was one of the reasons that caused an overvoltage during the first charge cycle owing to the activation phenomenon [22]. It was later found that there was a high charge transfer resistance at the interface between Li_2S and liquid electrolyte, which was lowered by coating the Li_2S particle with TiS_2 [23]. In situ coating of the solid electrolyte onto the Li_2S particle surface also enhanced the charged transfer resistance between the Li_2S particle and electrolyte, and thus reduced the overvoltage during the first scan [24]. These observations, including the results in this study, indicated that the overvoltage of the cell (or positive electrode) was reduced during the first scan owing to the complicated reaction among the components of the cell. It is also worth noting that a voltage of 3.0 V versus Li–In or 3.62 V versus Li/Li^+ was still sufficiently low to prevent the solid electrolyte from an oxidation reaction [25]; therefore, the oxidation reaction (or the charge capacity) observed in this study was attributed to the change from Li_2S to S. From the CV results, a cutoff voltage of 3.0–0.6 V versus Li–In was chosen to investigate the cyclic and C-rate performances of the all-solid cell to clarify the effect of MgS addition.

The voltage profiles and the cyclic performances of the cells employing Li_2S ($x=0$) and $Li_{1.7}Mg_{0.15}S$ are depicted in Fig. 4c–e. The initial Coulombic efficiency of the cells was higher than 95% and reached a stable value of higher than 99% after the tenth cycle. The first coulombic efficiency of the cell $x=0$ was about 104%. It is unusual if only the conversion Li_2S–S was counted. However, the oxidation of solid electrolyte might occur and cause the increase of CE in this case [26, 27]. The capacity of the cell with MgS addition was slightly lower than that without addition up to the 20^{th} cycle, but it became superior as the cycle number was increased. Capacities of the cells in Fig. 4e were calculated based on Li_2S. Theoretical capacities of $Li_{2-2x}Mg_xS$ were illustrated in supporting information part. The Coulombic efficiency of the cell containing MgS was also relatively stable during the cycling process. To quantify the effect of the addition of MgS on the electrochemical property of Li_2S, we calculated the "Li_2S conversion efficiency" of both the cells with and without the addition. We defined the "Li_2S conversion efficiency" as the ratio between the amount of electrochemically active Li_2S at cycle $n+1$ and cycle n. The result is depicted in the small inset in Fig. 4b. It was observed that during the first 10 cycles, the amount of electrochemically active Li_2S increased rapidly with the efficiency values in the range of 102%–115%. After the initial stage, the efficiency value of the sample with $x=0$ kept swinging in the range between 102%–100% until cycle number 25, then subsequently became lower than 100%. This result indicated that cell degradation commenced from cycle number 25. However, the cell that employed $Li_{1.7}Mg_{0.15}S$ exhibited a better performance with a higher Li_2S conversion efficiency value from cycle number 5. In addition, its conversion efficiency value was higher than 100% until cycle number 40, which meant that the cell capacity kept improving until cycle number 40 and subsequently started to decrease. CC–CV mode was also employed to charge–discharge the cell but the delivered capacities was unchanged. Therefore, ion and electron conduction paths were insufficient to connect all Li_2S particle inside the electrode. Improvement of electrode composite preparation method could be a solution to this issue.

EIS spectra of both cells before and after first cycle were illustrated in Fig. 4e–f. The internal resistance of both cells was reduced after the first cycle. Those results supported the observation in CV measurement which showed the oxidation peaks shifted from 2.13 to 1.95 V. The voltage gap in charge curves between first and second cycles also proved the reduction in internal resistance of the positive electrodes of the cells. The results from CV, EIS and charge–discharge tests revealed the interfacial reaction among the components of the cells which resulted in the reduction of cell resistance. The addition of MgS into Li_2S in this study resulted in the improvement of not only ionic conductivity but also the all-solid-state cell performance. Addition of Mo_6S_8, TiS_2 and Co_9S_8 into Li–S cells, which employed liquid electrolytes, could improve the cell performances because of the enhancement of both S conversion and polysulfide adsorption [28–30]. The dissolution of polysulfide doesn't occur in the all-solid-state cell so that boosting the Li_2S/S conversion should be the main reason for better performance of the cell with $x=0.15$ compared with that of $x=0$.

4 Conclusion

In this study, $Li_{2-2x}Mg_xS$ ($0 \le x \le 0.2$) was successfully prepared by planetary ball milling. Addition of MgS into Li_2S was able to improve its ionic conductivity owing to vacancy formation and the nanoionic effect. Li^+ ion movement in $Li_{2-2x}Mg_xS$ was driven by the vacancy mechanism at $0 < x \le 0.1$, while both the vacancy mechanism and nanoionic effect were found to be the governing factors at $0.1 < x \le 0.2$. Better cycling stability of the all-solid-state lithium–sulfur battery was also obtained with the addition

of MgS into Li_2S. The improvement of the ionic conductivity of Li_2S by the addition of MgS is expected to contribute to an improvement of the lithium metal battery because Li_2S has been recognized as an important component that forms a thin film on Li metal, which allows only Li ions to pass through and provides native insulation to an electron.

Acknowledgements This study was supported by the Advanced Low Carbon Technology Specially Promoted Research for Innovative Next Generation Batteries (JST-ALCA-SPRING, Grant No. JPMJAL1301) program of the Japan Science and Technology Agency. We thank Ms. Oshida Makiko and Mr. Shinoda Keisuke for their help with SEM-EDS measurements at National Institute for Materials Science (NIMS) Battery Research Platform.

Author contributions A. Matsuda & H. Muto: funding acquisition. N.H.H. Phuc.: experimental design, supervision, manuscript preparation. T. Maeda: data acquisition. K. Hikima: SEM – EDX data acquisition.

Compliance with ethical standard

Conflict of interest The authors declare that they have no competing interests

References

1. Fan L, Ma R, Yang Y, Chen S, Lu B (2016) Covalent sulfur for advanced room temperature sodium-sulfur batteries. Nano Energy 28:304–310
2. Qiang Z, Chen Y-M, Xia Y, Liang W, Zhu Y, Vogt BD (2017) Ultralong cycle life, low-cost room temperature sodium-sulfur batteries enabled by highly doped (N, S) nanoporous carbons. Nano Energy 32:59–66
3. Yun JH, Kim JH, Kim DK, Lee HW (2018) Suppressing polysulfide dissolution via cohesive forces by interwoven carbon nanofibers for high-areal-capacity lithium-sulfur batteries. Nano Lett 18:475–481
4. Pan H, Chen J, Cao R, Murugesan V, Rajput NN, Han KS, Persson K, Estevez L, Engelhard MH, Zhang J-G, Mueller KT, Cui Y, Shao Y, Liu J (2017) Non-encapsulation approach for high-performance Li–S batteries through controlled nucleation and growth. Nat Energy 2:813–820
5. Lin DC, Liu YY, Cui Y (2017) Reviving the lithium metal anode for high-energy batteries. Nat Nanotech 12:194–206
6. Tarascon JM (2010) Key challenges in future Li-battery research. Philos Trans A Math Phys Eng Sci 368:3227–3241
7. Su D, Zhou D, Wang C, Wang G (2018) Toward high performance lithium-sulfur batteries based on Li_2S cathodes and beyond: status, challenges, and perspectives. Adv Funct Mater 28:1800154
8. Beltran SP, Balbuena PB (2018) Formation of multilayer graphene domains with strong sulfur-carbon interaction and enhanced sulfur reduction zones for lithium-sulfur battery cathodes. Chemsuschem 11:1970–1980
9. Suzuki K, Kato D, Hara K, Yano T, Hirayama M, Hara M, Kanno R (2017) Composite sulfur electrode prepared by high-temperature mechanical milling for use in an all-solid-state lithium-sulfur battery with a $Li_{3.25}Ge_{0.25}P_{0.75}S_4$ electrolyte. Electrochim Acta 258:110–115
10. Rana M, Ahad SA, Li M, Luo B, Wang L, Gentle I, Knibbe R (2019) Review on areal capacities and long-term cycling performances of lithium sulfur battery at high sulfur loading. Energy Storage Mater 18:289–310
11. Hakari T, Hayashi A, Tatsumisago M (2017) Li_2S-Based solid solutions as positive electrodes with full utilization and superlong cycle life in all-solid-state Li/S batteries. Adv Sustain Syst 2017(1):1700017
12. Lorger S, Usiskin RE, Maier J (2018) Transport and charge carrier chemistry in lithium sulfide. Adv Funct Mater 29:1807688
13. Luo G, Zhao J, Wang B (2012) First-principles study of transition metal doped Li_2S as cathode materials in lithium batteries. J Renew Sustain Ener 4:063128
14. Phuc NHH, Yamamoto T, Muto H, Matsuda A (2017) Fast synthesis of Li_2S–P_2S_5–LiI solid electrolyte precursors. Inorg Chem Front 4:1660–1664
15. Spannenberger S, Miß V, Klotz E, Kettner J, Cronau M, Ramanayagam A, di Capua F, Elsayed M, Krause-Rehberg R, Vogel M, Roling B (2019) Annealing-induced vacancy formation enables extraordinarily high Li+ ion conductivity in the amorphous electrolyte 0.33 LiI + 0.67 Li_3PS_4. Solid State Ionics 341:115040
16. Sakuda A, Takeuchi T, Kobayashi H (2016) Electrode morphology in all-solid-state lithium secondary batteries consisting of $LiNi_{1/3}Co_{1/3}Mn_{1/3}O_2$ and Li_2S-P_2S_5 solid electrolytes. Solid State Ionics 285:112–117
17. Overton TL, Atkins PW, Rourke JP, Weller MT, Armstrong FA (2010) Shriver and Atkins' Inorganic Chemistry. Oxford University Press, Oxford
18. Takeuchi T, Kageyama H, Nakanishi K, Ogawa M, Ohta T, Sakuda A, Sakaebe H, Kobayashi H, Ogumi Z (2015) Preparation of Li_2S-FeS_x composite positive electrode materials and their electrochemical properties with pre-cycling treatments. J Electrochem Soc 162:A1745–A1750
19. Zhang B, Tan R, Yang L, Zheng J, Zhang K, Mo S, Lin Z, Pan F (2018) Mechanisms and properties of ion-transport in inorganic solid electrolytes. Energy Storage Mater 10:139–159
20. Xing Z, Tan G, Yuan Y, Wang B, Ma L, Xie J, Li Z, Wu T, Ren Y, Shahbazian-Yassar R, Lu J, Ji X, Chen Z (2020) Consolidating lithiothermic-ready transition metals for Li_2S-based cathodes. Adv Mater 32:e2002403
21. Ye H, Li M, Liu T, Li Y, Lu J (2020) Activating Li_2S as the lithium-containing cathode in lithium-sulfur batteries. ACS Energy Lett 5:2234–2245
22. Yang Y, Zheng G, Misra S, Nelson J, Toney MF, Cui Y (2012) High-capacity micrometer-sized Li_2S particles as cathode materials for advanced rechargeable lithium-ion batteries. J Am Chem Soc 134:15387–15394
23. Seh ZW, Yu JH, Li W, Hsu PC, Wang H, Sun Y, Yao H, Zhang Q, Cui Y (2014) Two-dimensional layered transition metal disulphides for effective encapsulation of high-capacity lithium sulphide cathodes. Nat Commun 5:5017
24. Jiao Z, Chen L, Si J, Xu C, Jiang Y, Zhu Y, Yang Y, Zhao B (2017) Core-shell $Li_2S@Li_3PS_4$ nanoparticles incorporated into graphene aerogel for lithium-sulfur batteries with low potential barrier and overpotential. J Power Sources 353:167–175
25. Adeli P, Bazak JD, Park KH, Kochetkov I, Huq A, Goward GR, Nazar LF (2019) Boosting solid-state diffusivity and conductivity in lithium superionic argyrodites by halide substitution. Angew Chem 58:8681–8686
26. Hakari T, Nagao M, Hayashi A, Tatsumisago M (2015) All-solid-state lithium batteries with Li_3PS_4 glass as active material. J Power Sources 293:721–725
27. Han F, Gao T, Zhu Y, Gaskell KJ, Wang C (2015) A battery made from a single material. Adv Mater 27:3473–3483
28. Pang Q, Kundu D, Nazar LF (2016) A graphene-like metallic cathode host for long-life and high-loading lithium–sulfur batteries. Mater Horiz 3:130–136

29. Chung S-H, Luo L, Manthiram A (2018) TiS_2–polysulfide hybrid cathode with high sulfur loading and low electrolyte consumption for lithium-sulfur batteries. ACS Energy Lett 3:568–573
30. Xue W, Shi Z, Suo L, Wang C, Wang Z, Wang H, So KP, Maurano A, Yu D, Chen Y, Qie L, Zhu Z, Xu G, Kong J, Li J (2019) Intercalation-conversion hybrid cathodes enabling Li–S full-cell architectures with jointly superior gravimetric and volumetric energy densities. Nat Energy 4:374–382